3-DoF Four-Cable-Driven Parallel Robot for Precision Align ment of Prefabricated Components

Wenjie Tang[1], Xiangsheng Chen[1],Silin Li[1], Yi Tan[1,2*]

[1]School of Civil and Transportation Engineering, The Shenzhen University, China.
[2]Sino-Australia Joint Research Center in BIM and Smart Construction, The Shenzhen University, Shenzhen, China.
1178492932@qq.com, xschen@szu.edu.cn, tanyi@szu.edu.cn,

Abstract –

Prefabricated buildings are increasingly adopted for their efficiency and environmental benefits. Howe ver, during hoisting and installation, accurate dockin g between bottom sleeves and pre-reserved steel bar regions is often hindered by limited visibility and poo r controllability of manual fine-tuning, reducing inst allation quality and efficiency. This paper proposes a four-cable-driven parallel robot system for precision alignment, enabling coordinated planar adjustment in two translations (x, y) and one rotation (yaw). The approach includes: (1) a scene-oriented CDPR config uration for suspended alignment, combining one pass ive main hoisting cable for gravity support and four actively actuated auxiliary cables for local planar an d yaw correction; (2) kinematic and static modeling with a wrench-feasible workspace analysis to determi ne the controllable region under tension constraints; and (3) trajectory-level simulation and prototype exp eriments to evaluate cable motion, tension feasibility, and alignment accuracy. Prototype experiments on a laboratory-scale prototype were conducted in 10 tria ls, achieving a 100% task success rate. The final plan ar error was 3.39 ± 1.05 mm and the final yaw error was 0.87 ± 0.59 deg. In 10 trials, all planar errors wer e below 5 mm, all yaw angle errors were less than 2°, and no cable slack was observed.

Keywords –

CDPR; Hoisting positioning; Prefabricated const ruction; Construction robotics

1 Introduction

With the increasing labor shortage in the constructio n industry and the rapid advancement of digital transfor mation, prefabricated construction has emerged as a mai nstream development approach due to its high efficienc y, environmental friendliness, and industrialized product ion [1]. Throughout the construction lifecycle of prefabric ated concrete structures, the hoisting and connection of p refabricated components play a decisive role in determin ing construction quality and project progress [2]. In partic ular, prefabricated column systems employing grouted s leeve connections require extremely high alignment acc uracy during installation, typically within millimeter-lev el tolerances [3].

However, current on-site hoisting still relies heavily on coarse crane positioning followed by manual fine adj ustment. After lifting, workers visually assess alignment and guide repeated micro-adjustments. This process is i nefficient, experience-dependent, and potentially unsafe under complex conditions [4–5]. Therefore, reducing ma nual intervention and enabling automated assembly of pr efabricated components has become a critical challenge in smart construction. In response, prefabricated constru ction has begun to incorporate an intelligent technology chain encompassing perception, planning, decision-maki ng, and motion control, aiming to improve the efficienc y, safety, and transparency of hoisting and on-site assem bly processes [6].

As a core enabling technology for intelligent percept ion, machine vision-based pose measurement provides a non-contact and high-precision solution for spatial local ization of prefabricated components [7]. In recent years, machine vision has demonstrated strong application pote ntial in industrial robotic grasping, autonomous driving , and unmanned aerial vehicle landing. In assembly align ment scenarios, monocular, stereo, or RGB-D vision sys tems can capture construction site imagery and, through feature extraction and pose estimation algorithms, outpu t six-degree-of-freedom pose information of components in real time [8]. For instance, Cheng et al. proposed a vis ion-based trajectory monitoring method for prefabricate d concrete component assembly, achieving pose measur ement accuracy of ±5 mm [9]. Long et al. integrated 3D p oint clouds and 2D images to develop an automated mea surement framework incorporating virtual trial assembly and alignment deviation analysis, attaining deviation ex traction accuracy below 1 mm and localization accuracy within 3 mm in both laboratory and field tests [10].

Despite these advances in pose perception, accurate s ensing alone is insufficient to realize automated alignme nt in construction environments. Conventional construct ion cranes typically operate in open-loop or low-bandwi dth control modes and lack fine-grained end-effector exe cution capability, making it difficult to directly respond to high-frequency, small-magnitude correction comman ds derived from visual feedback[11]. This highlights the necessity of a capable execution layer that can translate high-precision perception into continuous and controllable pose adjustment.

Cable-driven parallel robots (CDPRs) provide a promising solution to this execution challenge. Driven by multiple high-strength flexible cables, CDPRs achieve precise motion control of end-effectors through coordinated tension regulation and force distribution [12]. Compared with conventional rigid robotic systems, CDPRs offer advantages such as large workspaces, lightweight structures, and high flexibility, making them well suited to the requirements of prefabricated component alignment tasks [13]. Recent studies have explored CDPR applications in construction-related scenarios such as large-scale 3D printing and façade installation [14], demonstrating their potential for precise force–position hybrid control and fine pose adjustment.

Nevertheless, systematic research addressing pose adjustment execution for alignment deviation during prefabricated component hoisting remains limited, particularly with respect to automation level, system generality, and continuous controllability. To address this gap, this paper proposes a four-cable-driven parallel robot system for precision alignment of prefabricated components. Unlike conventional fully actuated CDPRs, the proposed system is designed for a suspended hoisting scenario, in which one passive main hoisting cable bears most of the gravitational load and four actively controlled auxiliary cables are responsible only for local alignment correction. This work develops a scene-oriented CDPR configuration and a closed-loop alignment process for automatic precision docking of suspended prefabricated columns. This study makes the following contributions: (1) A scene-oriented CDPR configuration is developed for suspended prefabricated-column alignment, in which one passive main hoisting cable provides primary gravity support and four active auxiliary cables perform local x-y-yaw correction. (2) A closed-loop alignment framework integrating pose perception, pose-error-based decision making, and cable actuation is established to enable automatic alignment rather than manual or open-loop adjustment. (3) Simulation and laboratory-scale prototype experiments validate that the proposed system can achieve repeatable alignment accuracy within practical installation tolerance requirements.

2 Literature Review

2.1 Hoisting Alignment Deviation Adjustment

Alignment deviation adjustment during the hoisting of prefabricated components has received relatively limited research attention, and a mature, general-purpose technical framework has yet to be established. Existing efforts mainly follow several representative approaches. Shen et al. proposed a guiding-frame-based positioning method for precast columns, where a limiting frame imposes geometric constraints on the pre-reserved rebars to guide the component into place during lowering; however, the automation level remains low and the process still relies on passive guidance and manual assistance[15]. Liu et al. developed a vision-guided robotic manipulator–assisted assembly method, in which an end-effector is inserted into the reserved holes and the component is pushed along a planned path to achieve alignment. Although this enables a perception–execution closed loop, it has so far been mainly demonstrated for slab-type components, and on-site deployment may be constrained by workspace and operating conditions[16]. Song et al. proposed the Hybrid Pose Adjustment robot, which coordinates multiple joints, cables, and thrusters to achieve pose leveling and swing suppression; nevertheless, the system is structurally complex and costly, with limited generality and rapid deployability[17]. Therefore, further exploration is still needed for execution-layer solutions that better balance deployability and continuous fine adjustment.

2.2 Applications of CDPRs in Construction

Benefiting from large workspaces, lightweight structures, and adjustable force–position capability, CDPRs have gradually advanced toward construction applications in recent years. Existing studies have explored CDPRs in façade installation, modular end-effector design, modeling and control for component installation, large-workspace vision-based control, and even complex brick construction [16], [18]–[21]. In addition, cost–benefit analysis has also been discussed for CDPR deployment in construction practice [22]. However, these studies do not directly address millimeter-level sleeve–rebar docking of suspended prefabricated columns through a lightweight four-cable execution layer driven by perception-based local pose correction.

3 Methodology

3.1 Problem Formulation and Assumptions

This study focuses on the fine alignment stage during the hoisting installation of prefabricated columns. At this stage, the component has been coarsely positioned by the crane, yet centimeter-level planar deviations and small yaw misalignment still need to be corrected before the final docking with pre-embedded reinforcement. Therefore, the process is formulated as a local pose correction problem under suspension constraints. The overall system configuration of the proposed cable-driven parallel robot for precision alignment is illustrated in Fig. 1.

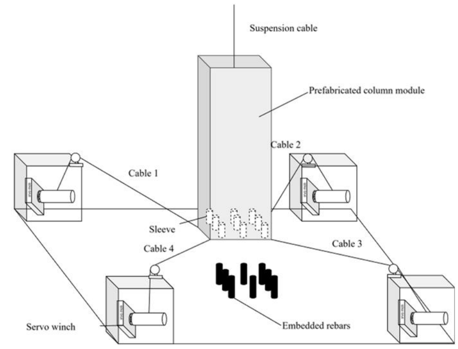

Figure 1. System configuration of the proposed cable-driven parallel robot for precision alignment.

The alignment objective is defined by a pose error vector

$$e = [\delta x,\ \delta y,\ \delta\psi]^T \tag{1}$$

where δx and δy denote the horizontal translational errors in the ground plane, and $\delta\psi$ represents the yaw misalignment between the component and the target reinforcement layout. The control goal is to drive e to zero through coordinated cable actuation.

The proposed system consists of one passive main suspension cable and four actively actuated adjustment cables. Unlike conventional fully actuated CDPRs, the main cable is not actively controlled and carries most of the component weight, while the four auxiliary cables are used only for local fine alignment during docking. The main cable provides gravity support, and the auxiliary cables generate controllable in-plane forces and moments for continuous planar and yaw correction. Accordingly, three controlled DoFs are considered: x, y, and yaw ψ.

The choice of these DoFs follows practical installation requirements. The critical acceptance targets mainly concern horizontal alignment between rebars and grouted sleeves and the in-plane axis orientation. The z direction is mainly governed by the crane and is not actively adjusted in the proposed lightweight four-cable system, while out-of-plane rotations are less critical for sleeve–rebar docking and are partly suppressed by the suspension configuration. Therefore, focusing on x, y, and yaw provides a practical strategy for the fine alignment stage.

Finally, the alignment process is assumed to be quasi-static, as cable-length adjustments are executed at low speed to ensure safety and controllability. Under this assumption, the task is treated as a quasi-static pose correction problem for the subsequent kinematic mapping and static feasibility analysis. This assumption is intended only for the final low-speed docking stage, where large-amplitude oscillations are not considered.

3.2 Kinematic Mapping from Pose Error to Cable-Length Commands

This section presents the kinematic mapping that converts the pose error provided by the perception module, $e = [\delta x,\ \delta y,\ \delta\psi]^T$ into executable cable-length commands for the four-cable adjustment subsystem. The mapping is established from the geometric relationship between the fixed anchor points and the cable attachment points on the prefabricated module, enabling continuous and controllable correction of planar translation and yaw misalignment.

3.2.1 Geometric Model and Cable-Length Computation

A world frame $\{W\}$is defined on the worksite, and a body-fixed frame $\{B\}$is attached to the module. Let $\mathbf{a}_i \in \mathbb{R}^3$denote the position of the i-th cable anchor point expressed in $\{W\}$, and $b_i \in \mathbb{R}^3$denote the corresponding cable attachment point expressed in $\{B\}$, where $i = 1,2,3,4$. Under the 3-DoF assumption, the module pose is parameterized by

$$q = [x,\ y,\ \psi]^T \tag{2}$$

where x and y represent planar translation and ψ denotes yaw rotation about the vertical axis. As shown in Figure 2.

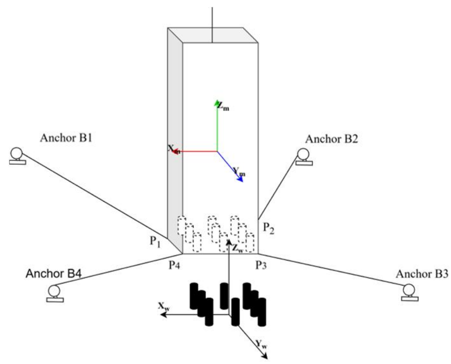

Figure 2. Geometric modeling and coordinate definition of the suspended prefabricated column.

The body-to-world rotation is therefore described by

$$\mathrm{R}_z(\psi) = \begin{bmatrix} \cos\psi & -\sin\psi & 0 \\ \sin\psi & \cos\psi & 0 \\ 0 & 0 & 1 \end{bmatrix}. \tag{3}$$

Let the module reference point in $\{W\}$be $p = [x,\ y, z_0]^T$ where $z_0$is treated as constant during fine alignment. The world position of the i-th attachment point is then computed as

$$s_i(q) = p + R_z(\psi)b_i \tag{4}$$

Accordingly, the i-th cable vector and cable length are given by

$$\mathrm{c}_i(\mathrm{q}) = \mathrm{a}_i - \mathrm{s}_i(\mathrm{q}), l_i(\mathrm{q}) = \| \mathrm{c}_i(\mathrm{q}) \|_2 \tag{5}$$

3.2.2 Geometric First-Order Mapping for Fine Alignment

In the fine alignment stage, the required corrections are typically small. Hence, the relationship between incremental pose correction and cable-length variation can be approximated by a first-order model:

$$\Delta l \approx J(q)\Delta q, \quad (6)$$

where $\Delta l = [\Delta l_1, \Delta l_2, \Delta l_3, \Delta l_4]^T$, and $J(q) \in \mathbb{R}^{4\times3}$ is the cable-length Jacobian. Let $\hat{u}_i = c_i / \| c_i \|_2$ denote the unit direction of the i-th cable. The corresponding Jacobian terms can be expressed as

$$\frac{\partial l_i}{\partial x} = -\hat{u}_i^T \begin{bmatrix}1\\0\\0\end{bmatrix}, \frac{\partial l_i}{\partial y} = -\hat{u}_i^T \begin{bmatrix}0\\1\\0\end{bmatrix}, \quad \frac{\partial l_i}{\partial \psi} = -\hat{u}_i^T \left(\frac{\partial R_z(\psi)}{\partial \psi} b_i\right) \quad (7)$$

Equations (6)–(7) provide an efficient computation of the cable-length corrections required to realize a desired pose correction Δq. In practice, $J(q)$ can be updated using the current pose estimate, allowing real-time conversion of perception errors into executable length commands.

3.2.3 Cable-Length Command Generation

Given the measured pose error e, the desired correction can be defined as $\Delta q = -e$. Since the system is redundantly actuated in terms of cable count but controls 3DoFs, cable-length commands can be generated either (i) by directly evaluating (5) at the updated pose $q + \Delta q$, or (ii) by computing Δl via the differential mapping in (6) and integrating it over time. To ensure numerical stability for small-range alignment, this study adopts the differential mapping and constructs cable-length trajectories as

$$l_{cmd}(t) = l_0 + \Delta l(t), t \in [0, T] \quad (8)$$

where $\mathbf{l}_0$ denotes the initial cable lengths at the measured initial pose and T is the prescribed alignment duration. The resulting cable-length commands are subsequently checked against tension feasibility constraints, as described in Section 3.3.

3.3 Static Feasibility Analysis Under Tension Constraints

While the kinematic mapping in Section 3.2 determines the cable-length variations required for pose correction, the physical feasibility of these commands must be verified through static tension constraints. Since cable-driven systems can only transmit tensile forces, all cables must remain in tension throughout the fine alignment process to ensure controllability and structural safety.

3.3.1 Quasi-Static Force Equilibrium

Under the quasi-static assumption introduced in Section 3.1, inertial and dynamic coupling effects are neglected, and the suspended module is assumed to be in static equilibrium at each intermediate pose. Let $T = [T_1, T_2, T_3, T_4]^T$ denote the tensions in the four adjustment cables, and let T_s denote the tension in the main suspension cable. The force equilibrium condition of the module can be expressed as

$$\sum_{i=1}^{4} T_i \hat{u}_i + T_s \hat{u}_s + W = 0, \quad (9)$$

where $\hat{u}_i$ and $\hat{u}_s$ are the unit direction vectors of the adjustment cables and the suspension cable, respectively, and $W = [0, 0, -mg]^T$ represents the gravitational force acting on the module.

Similarly, moment equilibrium about the module reference point must be satisfied:

$$\sum_{i=1}^{4} r_i \times (T_i \hat{u}_i) = 0 \quad (10)$$

where r_i denotes the position vector of the i-th cable attachment point relative to the reference point. Since the suspension cable is assumed to pass through or near the reference point, its contribution to the moment equilibrium is neglected in the fine alignment stage. Equations (9)–(10) collectively define the static force–moment balance required for feasible pose correction.

3.3.2 Tension Feasibility Conditions

For a given pose and corresponding cable geometry, the static equilibrium equations generally admit infinitely many tension distributions due to actuation redundancy. However, only solutions satisfying unilateral tension constraints are physically admissible:

$$T_i \geq T_{\min}, i = 1, \ldots, 4. \quad (11)$$

Here, $T_{\min}$ is a prescribed minimum tension to prevent cable slack and ensure stable force transmission. In practice, $T_{\min}$ is selected based on cable properties, winch characteristics, and safety considerations.

A pose is defined as tension-feasible if there exists at least one tension vector T satisfying both the equilibrium equations (9)–(10) and the inequality constraints (11). The collection of all such poses constitutes the tension-feasible workspace (TFW) of the system. During fine alignment, the planned pose trajectory must remain within this workspace to guarantee continuous controllability.

3.3.3 Tension Distribution Strategy

To obtain a unique and stable tension solution, an additional optimization criterion is introduced. In this study, the tension distribution is determined by minimizing the overall tension level while enforcing a minimum tension constraint:

Under the quasi-static assumption, the force and moment equilibrium conditions can be compactly expressed as

$$A(q)T = b(q) \quad (12)$$

where $\mathbf{T} = [T_1, T_2, T_3, T_4]^T$ denotes the tension vector of the four adjustment cables, $A(q)$ is the equilibrium coefficient matrix determined by the cable geometry and attachment locations, and $b(q)$ represents the external load vector dominated by gravity. The tension in the main suspension cable is treated as a known quantity determined by weight balance and is not included in the optimizati on variables.

To resolve the redundancy, the tension distribution is formulated as the following constrained optimization problem:

$$T^{*} = argmin_{T} \parallel T \parallel_{2}^{2} \quad s.t. A(q)T = b(q), \quad T_{i} \geq T_{min}, i = 1, \ldots, 4. \tag{13}$$

This formulation promotes balanced cable loading while preventing cable slack through the minimum tension constraint $T_{\min}$. The resulting tension solution is subsequently used for tension feasibility verification and for generating tension-related outputs in the simulation results. By combining the kinematic mapping in Section 3.2 with the static feasibility analysis presented here, the proposed system ensures that the pose correction commands are not only geometrically valid but also physically realizable under realistic hoisting and cable constraints.

4 Results and Validation

4.1 Simulation Setup and Parameters

Simulation studies were conducted in a 3D numerical environment to evaluate the proposed four-cable alignment system. The suspended column was modeled as a 300 mm × 300 mm × 400 mm rigid body with a mass of 90 kg, attached to a passive main cable and four active cables for planar and yaw correction. The maximum cable speed and acceleration were set to 0.02 m/s and 0.04 m/s², respectively, and trapezoidal motion profiles were used for smooth cable-length commands.

The tension-feasible workspace was evaluated under the quasi-static model by discretizing the planar workspace and solving the equilibrium equations at each sampled pose. A pose was considered feasible only when all cable tensions remained within 10–100 N. As shown in Figure 4, the feasible region occupies only part of the geometric workspace. The central region shows lower peak tension and higher manipulability, while boundary regions require larger cable forces and provide weaker control authority. These results support feasibility-aware alignment planning.

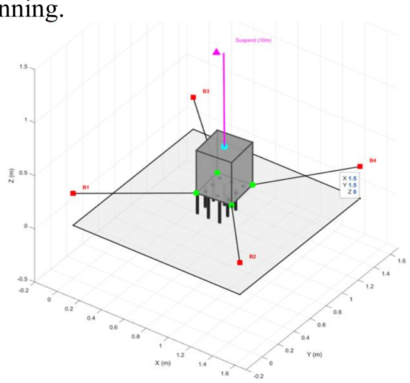

Figure 3. Alignment System Simulation & 3D Model

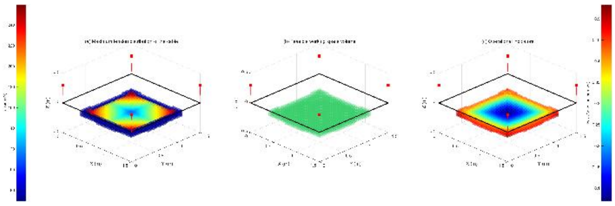

Figure 4. Workspace analysis results: (a) maximum cable tension distribution; (b) tension-feasible workspace; (c) manipulability index distribution.

4.2 Trajectory-Level Simulation Results

Figure 5 summarizes the trajectory-level simulation results. The alignment trajectory remains inside the feasible workspace, and the x, y, and yaw errors converge smoothly toward the target pose under the quasi-static assumption.

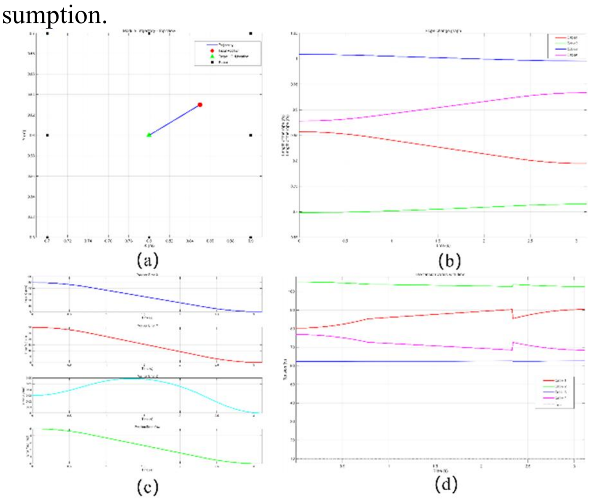

Figure 5. Simulation results: (a) planar alignment trajectory; (b) cable-length variations; (c) time histories of pose errors; (d) cable tension variations.

The cable-length commands remain continuous throughout the alignment process, and all cable tensions remain above the minimum threshold. These simulation results provide feasibility support for the subsequent hardware prototype validation.

4.3 Prototype Experiment and Results

4.3.1 Experimental Platform

Figures 6–8 present the prototype experimental system, including the laboratory setup, the perception-control architecture, and the cable actuation module. A laboratory-scale prototype was built for the prototype experiment. The prototype used a reduced-scale 15 kg column model due to laboratory constraints, whereas the 90 kg model was used in simulation to represent a heavier suspended component. The system comprises four Inovance servo drivers, four Inovance servo motors, one H5U PLC, and an upper computer. A threaded drum was mounted on each motor shaft for orderly cable winding. The actuation modules were installed on an aluminum frame and connected through fixed pulleys and universal guide pulleys. The system manipulated a suspended prefabricated-column model beneath a tower-crane mock-up. Pose estimation was performed using an Intel RealSense D455 with a ChArUco board and a depth-assisted PnP algorithm. Cable tension feasibility was monitored indirectly through servo-state feedback during the experiments.

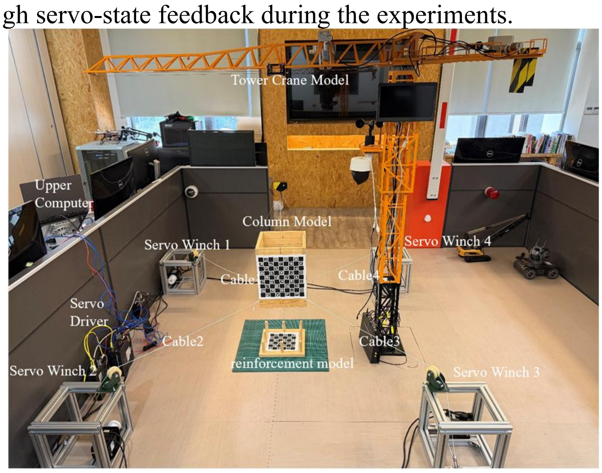

Figure 6. Laboratory prototype of the proposed four-cable-driven alignment system.

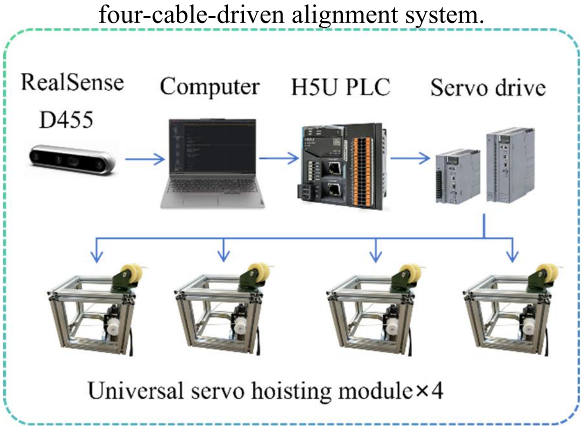

Figure 7. Perception-control architecture of the experimental system.

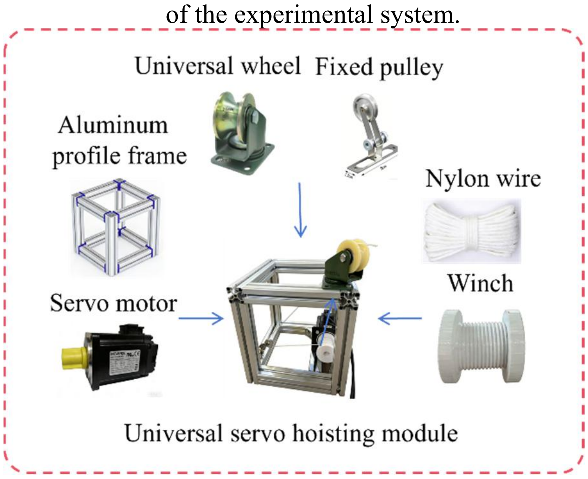

Figure 8. Composition of a cable actuation module.

4.3.2 Experimental Procedure

Pose estimation during the prototype experiment was performed at 30 Hz by the Intel RealSense D455 using the ChArUco board and a depth-assisted PnP algorithm. Due to space limitations, a 300 mm × 300 mm × 400 mm prefabricated-column model with a mass of approximately 15 kg was used, and its bottom contains eight 30 mm holes corresponding to an embedded rebar mock-up with eight 20 mm cylindrical bars. A reference installation pose was first established and measured by a Trimble X7 laser scanner. For each trial, the suspended column was manually displaced to a radial initial position around the reference pose, including upper, lower, left, right, diagonal, and additional random directions, with planar offsets of approximately 5 to 8 cm. The controller first adjusted the cable lengths to reduce the yaw error toward zero and then performed planar alignment. After convergence, the scene was scanned again by the Trimble X7, and the final pose was extracted from segmented and preprocessed point clouds with fitted planar surfaces. Planar error was defined as the Euclidean offset between the final measured column reference point and the reference installation pose in the horizontal plane, while yaw error was defined as the absolute yaw-angle difference relative to the reference pose. A trial was considered successful if the docking task was completed without cable slack and the final pose remained within the predefined alignment tolerance. The above process was executed in the proposed perception–decision–control loop using real-time pose updates from the vision module. The alignment process was terminated when the planar error fell below 5 mm and the yaw error fell below 2 deg.

4.3.3 Experimental Results

Across 10 trials, all docking tasks were successfully completed, corresponding to a 100% task success rate under the current laboratory conditions. The final planar error was 3. 39 ± 1.05 mm and the final yaw error was 0. 87 ± 0.59 deg. According to industry installation requirements, the steel-bar alignment error should remain below 5 mm to satisfy the assembly tolerance. This requirement was therefore adopted as the planar acceptance criterion in the prototype experiments. All planar errors were below 5 mm, all yaw errors were below 2 deg. The alignment time in all trials was below 30 s. Cable tension feasibility was monitored indirectly through servo-state feedback during the experiments, and no cable slack was observed. Figure 9 compares the initial and final bottom reference point positions in the prototype trials. Although the initial positions show noticeable deviations, all final aligned positions converge into the 5 mm installation tolerance region required for steel-bar alignment, indicating that the proposed system can effectively correct the initial planar misalignment and achieve repeatable docking accuracy. These results indicate that the proposed system is capable of automatically correcting initial planar misalignment under closed-loop feedback, rather than relying on manual micro-adjustment during the final docking stage.

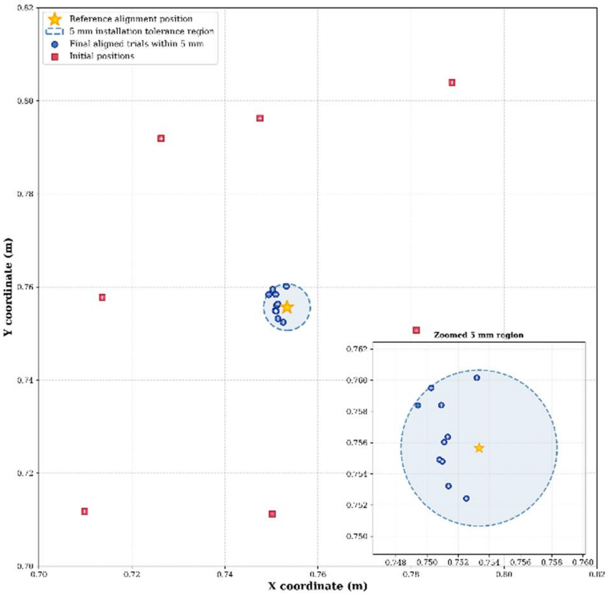

Figure 9. Top-view distribution of initial and final alignment positions.

The red squares denote the initial positions before alignment, and the blue circles denote the final positions after automatic alignment. The star indicates the reference alignment position, and the dashed circle represents the 5 mm installation tolerance region required for steel-bar alignment. The figure shows that the proposed system drives dispersed initial misalignments into the required tolerance region with good repeatability.

4.4 Discussion

The prototype results support the quasi-static assumption adopted in this study for the final low-speed docking stage. In a conventional hoisting scenario without auxiliary alignment cables, suspended components may exhibit prolonged oscillation under wind load and other disturbances. In contrast, when four auxiliary cables are introduced and maintained under positive tension, the prefabricated column is constrained around a local equilibrium state. Under the current laboratory conditions, prototype observations showed that small perturbations decayed rapidly and had limited influence on the final alignment result. These results suggest that the proposed perception–decision–control loop can achieve stable convergence for final suspended alignment, although a full dynamic analysis remains for future study.

Several practical factors and limitations still deserve attention. The auxiliary cables used in the current prototype are nylon ropes with a certain degree of elasticity. Although this elasticity may introduce small errors in a single adjustment step, it also provides a buffering effect against vibration. In the proposed visual closed-loop alignment process, residual errors caused by cable elasticity can be progressively reduced through repeated pose measurement and winch adjustment. Since the cables remain under positive tension after each step and are already in an elongated state, the additional elasticity-induced error is reduced in subsequent corrections. As observed in the prototype experiments, cable elasticity did not prevent stable convergence or successful docking. Winch synchronization is also explicitly considered in the current CDPR control algorithm by constraining the maximum rotational speed and coordinating synchronous start-stop behavior among the four winches, which helps avoid obvious desynchronization in the prototype experiments.

The present validation is limited to a laboratory-scale prototype. In addition, cable interference was not treated as a dominant issue because the current scenario focuses on the installation of a single prefabricated column in a relatively open area around the embedded rebars, where four servo winch modules are arranged approximately 1–2 m around the target region to facilitate planar correction and yaw adjustment. Visual sensing has been integrated into the system to estimate the relative alignment error between the prefabricated column and the embedded rebars, which is then converted into cable-length adjustments through the CDPR controller. Future work will further investigate swing dynamics, disturbance sensitivity, equipment-layout optimization, and multi-column deployment in more realistic construction environments.

Table 1 shows that the proposed four-cable CDPR provides a balanced solution for suspended docking, combining high precision potential with moderate cost and good deployability.

Table 1. Brief comparison of alignment solutions

Method	Precision	Cost	Deployability
Crane-based fine control	Low	Low	High
Rigid manipulator	High	High	Medium
Hybrid alignment robot	High	High	Medium
Proposed four-cable CDPR	High	Medium	High

5 Conclusion

This study proposed a four-cable-driven parallel robot for fine alignment of prefabricated columns under suspended conditions. A kinematic mapping was developed to convert perception-based pose errors into cable-length commands, and a quasi-static tension feasibility model was used to ensure physically admissible actuation. Simulation studies verified the feasible workspace and conti nuous cable-length and tension evolution during alignment. Prototype experiments on a laboratory-scale prototype further validated the approach in 10 trials, corresponding to a 100% task success rate. The final planar error was 3.39 ± 1.05 mm and the final yaw error was 0.87 ± 0.59 deg. In 10 trials, all planar errors were below 5 mm, all yaw angle errors were less than 2°, and no cable slack was observed. These results provide laboratory-scale validation that the proposed system can achieve stable and accurate suspended alignment.

Future work should further address stronger disturbances, longer cable spans, anchor-point arrangement, winch synchronization under larger-scale deployment, and direct tension sensing in more realistic construction environments.

References

[1] L. Parisi and S. Donyavi. Modular momentum: Assessing the efficacy of modular construction in alleviating the UK housing crisis. Discov Appl Sci, 6:548, 2024.

[2] R. Martins, R.D. Carmo, H. Costa, and E. Júlio. A review on precast structural concrete walls and connections. Advances in Structural Engineering, 26:2600–2620, 2023.

[3] E. Ouda and M. Haggag. Automation in modular construction manufacturing: A comparative analysis of assembly processes. Sustainability, 16:9238, 2024.

[4] T. Cheng and J. Teizer. Modeling tower crane operator visibility to minimize the risk of limited situational awareness. Journal of Computing in Civil Engineering, 28:04014004, 2014.

[5] H. Sadeghi, C.M. Cheung, A. Yunusa-Kaltungo, and P. Manu. A systematic review of occupational safety and health in modular integrated construction. Safety Science, 189:106897, 2025.

[6] Y. Zhao, C. Cao, Z. Liu, and E. Mu. Intelligent control method of hoisting prefabricated components based on internet-of-Things. Sensors, 21:980, 2021.

[7] J. Guan, Y. Hao, Q. Wu, S. Li, and Y. Fang. A survey of 6DoF object pose estimation methods for different application scenarios. Sensors, 24:1076, 2024.

[8] V. Lepetit, F. Moreno-Noguer, and P. Fua. EPnP: An accurate O(n) solution to the PnP problem. International Journal of Computer Vision, 81:155–166, 2009.

[9] Y. Cheng, F. Lin, W. Wang, and J. Zhang. Vision-based trajectory monitoring for assembly alignment of precast concrete bridge components. Automation in Construction, 140:104350, 2022.

[10] L. Long, W. Liu, S. Xu, P. Shi, C. Zhang, and L. Deng. Automated alignment deviation measurement for precast concrete assembly using point cloud-image fusion. Automation in Construction, 180:106540, 2025.

[11] S.M. Bagheri. Automated safety and practicality enhancement of lift plans in modular construction. PhD Thesis, University of Alberta, Canada, 2024.

[12] K. Joyo, H. Yuan, J. Wu, W. Xu, and H. Yue. Advancements and theoretical foundations of cable-driven parallel robots: A comprehensive overview. Chinese Journal of Mechanical Engineering, 2025.

[13] Z. Shao, G. Xie, Z. Zhang, and L. Wang. Design and analysis of the cable-driven parallel robot for cleaning exterior wall of buildings. Journal of Building Engineering, 2021.

[14] K. Iturralde. Cable-driven parallel robot for curtain wall module installation. Automation in Construction, 2022.

[15] L. Shen, H. Wei, Y. Liang, et al. Precise positioning technology for hoisting PC columns of prefabricated buildings. Building Construction, 42(09):1671–1673, 2020.

[16] Y. Liu, X. Zhang, H. Wang, and J. Li. Automatic assembly of prefabricated components based on vision-guided robot. Automation in Construction, 158:105040, 2024.

[17] C. Song, X. Li, Q. Du, R. Jiang, and Q. Shen. Hybrid pose adjustment (HyPA) robot design for prefabricated module control in modular construction assembly. Automation in Construction, 168:105798, 2024.

[18] K. Iturralde, A. Maldonado, and W. Pan. A cable-driven parallel robot with a modular end effector for the installation of curtain wall modules. Automation in Construction, 2020.

[19] Y. Liu and A. Maldonado. Dynamic modeling, trajectory optimization, and linear control of cable-driven parallel robots for automated panelized building retrofits. Automation in Construction, 2025.

[20] S. Dallej, A. Pott, and F. Chaumette. Modeling and vision-based control of large-dimension cable-driven parallel robots using a multiple-camera setup. IEEE Transactions on Robotics, 2019.

[21] P. Wu, K. Iturralde, and W. Pan. CU-brick cable-driven robot for automated construction of complex brick structures: From simulation to hardware realization. Automation in Construction, 2018.

[22] Y. Hu, W. Pan, and K. Iturralde. A simple framework for the cost–benefit analysis of single-task construction robots based on a case study of a cable-driven facade installation robot. Automation in Construction, 2020.